

# Inverse optically-induced ring currents in ring-shaped molecules

Krishna Reddy Nandipati,<sup>\*,†,‡,§</sup> Sudip Sasmal,<sup>\*,†,§</sup> and Oriol Vendrell<sup>\*,†,¶</sup>

<sup>†</sup>*Theoretische Chemie, Physikalisch-Chemisches Institut, Universität Heidelberg, Im Neuenheimer Feld 229, 69120 Heidelberg, Germany*

<sup>‡</sup>*Department of Chemistry, Indian Institute of Technology Madras, 600036 Chennai, India*

<sup>¶</sup>*Interdisciplinary Center for Scientific Computing, Universität Heidelberg, Im Neuenheimer Feld 205, 69120 Heidelberg, Germany*

<sup>§</sup>*Contributed equally to this work*

E-mail: knandipati@iitm.ac.in; sudip.sasmal@pci.uni-heidelberg.de;  
oriol.vendrell@uni-heidelberg.de

## Abstract

Permanent electronic ring currents can be supported within a manifold of  $\Gamma_E$  degenerate excited electronic states as  $E_{\pm} = E_x \pm iE_y$  excitations. This requires at least a 3-fold-symmetry rotational axis or higher, and includes the subclass of ring-shaped molecules. In [Phys. Rev. Res. **3**, L042003 (2021)] we showed the existence of inverse-current manifolds, where the direction of the electronic ring-current in each degenerate state  $E_{\pm}$  is opposite to the circular polarization of the generating light-fields. This phenomenon can be traced back to vibronic effects, namely the exchange of orbital angular momentum between the circulating electrons and vibrational modes with the required symmetry. Here we consider the case of fixed nuclei and find that ring-shaped molecular systems can possess inverse-current manifolds on a purely electronic-structure basis, i.e. without intervention of vibronic coupling. The effect is illustrated and explained first on a simple tight-binding model with cyclic symmetry, and then

considering the *ab initio* electronic structure of benzene and sym-triazine. A framework for discriminating regular- and inverse-current  $\Gamma_E$  manifolds in molecules using quantum chemistry calculations is provided.

The generation and control of electronic currents in ring-shaped molecules<sup>1–10</sup> and materials thereof<sup>11–13</sup> using polarized light fields have gained considerable interest due to their potential applications in optoelectronics,<sup>14</sup> for example, as ultrafast switching units.<sup>13</sup> Recent advances in the knowledge of ring currents and their generation using either circularly polarized laser pulses<sup>4,10,15,16</sup> or a pair of linearly polarized laser pulses,<sup>7,8,17</sup> in particular, in the aromatic molecular systems such as benzene and Mg-porphyrin (MgPh), pave the way for their potential applications as molecular switches. Also, with the improvements in the technologies for atom-by-atom fabrication of planar clusters such as cyclo[18]-carbon,  $C_{18}$ ,<sup>18</sup> the generation and control of the currents in such systems may lead to unforeseen applications in the field of molecular electronics. The experimental advances in femto- and attosecond laser technology<sup>19,20</sup> have further motivated theoretical investigations on electronic ring currents and their generation, in time-scales comparable to the fastest vibrational dynamics in molecules,<sup>9,10,21</sup> mainly fixing nuclear geometry,<sup>1–9,11–13,22,23</sup> i.e. within the Born-Oppenheimer (BO) approximation. In these studies, symmetry as a selection criteria for molecular systems to present ring currents is often exploited – the requirement of the presence of doubly degenerate ( $E$ ) electronic states with finite angular momentum, present in those molecular systems that have at least 3-fold or higher symmetry axis ( $C_{n \geq 3}$ ) in order to support ring currents. However, the fundamental role of symmetry in understanding the properties of generated ring currents remains unexplored.

Recent theoretical studies on the generation of ring currents have extended to include vibronic coupling effects, i.e. going beyond the BO regime.<sup>15,16,24</sup> These studies<sup>16,24</sup> showed that nonadiabatic couplings in molecules play crucial role in determining the extent of electronic ring current achieved by the CP pulses – the stronger the nonadiabatic interaction the lower the net generated current in a given molecular eigenstate, owing to the strong coupling between angular momenta of the electrons and nuclei. In other words, the right- and left-circulation directions of the electron represented by the  $E$  state become mixed by the coupling to the nuclear vibrations, and this coupling sets an intrinsic limit to the maximum amount of current that the molecular system can

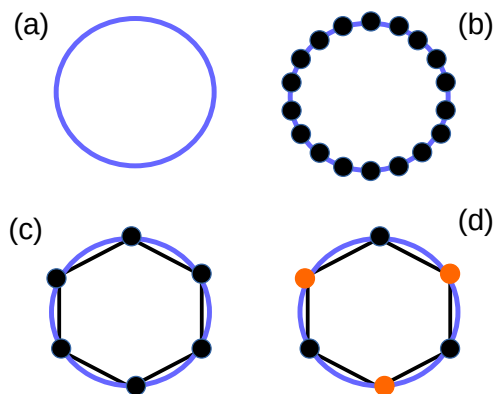


Figure 1: The ring with  $C_\infty$  rotational axis of symmetry (a) is discretized into rings with axes of symmetry  $C_{18}$  (b),  $C_6$  (c) and  $C_3$  (d). The black dots in (b-d) represent C-H sites and the orange dots in (d) represent hetero-atom sites (N, in the present work).

support in an eigenstate. The more surprising and even intriguing aspect of the generated currents under nonadiabatic couplings is that the direction of the currents does not necessarily have to be the same as the polarization direction of the applying CP pulses.<sup>16</sup> Such currents are referred to as inverse ring currents and are a result of spontaneous symmetry-breaking effects in molecules, the so-called Jahn-Teller effects.

In this work, we show that, even within the BO approximation (i.e. fixing nuclear geometry), such inverse ring currents do exist in molecules that inherently support ring currents and they can be generated using CP pulses. The origin of such currents is elucidated in the context of a reduction in molecular symmetry. Also, we shed light on the suppression in the amount of generated currents using arguments based on the symmetry-lowering of a molecular system relative to that of a correspondingly higher rotational axis of symmetry. Our target systems of interest to study these nontrivial properties of the currents are representative planar ring-shaped molecular systems, for example, benzene and 1,3,5-sym triazine, owing to their high symmetry ( $C_{n \geq 3}$ ) and wide applicability as building blocks in optoelectronic materials. To illustrate the effects of symmetry-lowering on the generation of currents in ring-shaped molecules, we consider a model of finite-site ring systems i.e., the discretized versions of an infinitely-fold symmetric ring (cf. Figure 1) described by tight-binding Hamiltonians. These discrete rings represent a class of aromatic molecules with

different symmetries, each possessing at least  $C_3$  principal axis of symmetry as necessary for the manifestation of electronic ring currents. The rings lie on the  $(x,y)$ -plane and the laser field is assumed to propagate along the  $z$ -direction, i.e. the principal axis of symmetry. The (discretized) model ring-shaped systems under consideration encompass a 6(CH)-site system and a 3(CH)-3(N)-site system. These models serve as representations for homocyclic  $C_6H_6$  systems and heterocyclic 1,3,5 sym- $C_3N_3H_3$ , (cf. Fig. 1 and its caption).

*Hückel model* – The tight-binding Hamiltonian for a ring with a  $C_n$  symmetry axis perpendicular to the  $(x,y)$ -plane reads

$$\hat{H} = -t \left( \sum_{s=0}^{n-1} |\chi_s\rangle \langle \chi_{s+1}| + \text{h.c.} \right) \quad \text{with } |\chi_n\rangle \equiv |\chi_0\rangle \quad (1)$$

with transfer integral  $t > 0$ . The eigenstates of the tri-diagonal Hamiltonian read

$$|\phi_k\rangle = \frac{1}{\sqrt{n}} \sum_{s=0}^{n-1} e^{i\varphi_s k} |\chi_s\rangle, \quad (2)$$

where  $k$  is an integer and  $\varphi_s = 2\pi s/n$  is the angle of the  $|\chi_s\rangle$  basis site around the ring. For  $n$  odd,  $k$  takes values in the interval  $[-(n-1)/2, \dots, (n-1)/2]$  and for  $n$  even,  $k$  takes values in the interval  $[-n/2, \dots, n/2]$ . In the latter case,  $|\phi_{-n/2}\rangle$  and  $|\phi_{n/2}\rangle$  are linear dependent and the highest energy eigenstate of  $H$  is real-valued and non-degenerate. The proper eigenstate is defined by taking  $|\phi_{n/2}\rangle \rightarrow (|\phi_{-n/2}\rangle + |\phi_{n/2}\rangle)/2$ .

The states (2) are discrete analogs of the eigenstates of the particle on a ring

$$\psi_q(\varphi) = \frac{1}{\sqrt{2\pi}} e^{iq\varphi}, \quad (3)$$

which are eigenstates of the angular momentum perpendicular to the  $(x,y)$  plane,  $\hat{l}_z = -i\hbar\partial_\varphi$ , with eigenvalues  $\hbar q$  and quantum number  $q \in \mathbb{Z}$ . The in-plane angular momentum of the tight-binding

states (2) follows analogously

$$\begin{aligned}
L_{k,j} &= \langle \phi_k | \hat{l}_z | \phi_j \rangle \\
&= \frac{1}{n} \sum_{r=0}^{n-1} \sum_{s=0}^{n-1} e^{-i\varphi_s k} e^{i\varphi_r j} \langle \chi_s | \hat{l}_z | \chi_r \rangle \\
&= 2\hbar d \sin\left(\frac{2\pi k}{n}\right) \delta_{k,j}.
\end{aligned} \tag{4}$$

The last line in Eq. (4) is reached using the matrix elements of the in-plane angular momentum in the localized basis,

$$\begin{aligned}
\langle \chi_s | \hat{l}_z | \chi_r \rangle &= -i\hbar \langle \chi_s | \frac{\partial}{\partial \varphi} | \chi_r \rangle \\
&= -i\hbar d (r-s) \delta_{1,|r-s|},
\end{aligned} \tag{5}$$

where  $d = \langle \chi_s | \frac{\partial}{\partial \varphi} | \chi_{s+1} \rangle$  is the matrix element of the differential operator  $\partial_\varphi$  between two consecutive localized sites of the tight-binding system.  $d$  is a system-dependent one-electron integral. It can be numerically evaluated once a particular localized basis is chosen, or alternatively fitted empirically. Here, we leave this parameter unspecified and give the angular momenta in units of  $d$ .

The current density on the ring follows from the continuity equation<sup>25</sup> and reads

$$j(\varphi, t) = \frac{1}{I} \Re\{\phi^*(\varphi, t) \hat{l}_z \phi(\varphi, t)\}, \tag{6}$$

where  $I = m_e R^2$  is the moment of inertia with radius  $R$  and  $\phi(\varphi, t) = \sum_k c_k(t) \phi_k(\varphi)$  is the state of the system in the angular momentum basis (2). Defining the electron *ring current* as the integrated

current density around the ring<sup>24</sup> one arrives at

$$\begin{aligned}
C(t) &= \int_0^{2\pi} j(\varphi, t) d\varphi \\
&= \frac{2\hbar d}{I} \sum_k |c_k(t)|^2 \sin\left(\frac{2\pi k}{n}\right) \\
&= \frac{1}{I} \sum_k |c_k(t)|^2 L_{k,k},
\end{aligned} \tag{7}$$

where  $L_{k,k}$  is the angular momentum in Eq. (4).

*Interaction with CP light* – We describe the interaction between the ring system and CP light propagating along the  $z$ -direction (i.e. along the principle axis of symmetry) in the electric dipole approximation, and treat electromagnetic radiation classically. Hence, the electric field of the CP light in the plane of the ring assumes the form

$$\vec{E}(t) = \varepsilon (\vec{u}_x \cos(\omega t + \theta_x) + \vec{u}_y \cos(\omega t + \theta_y)) \tag{8}$$

where  $\varepsilon$  and  $\omega$  are the amplitude and carrier frequency, respectively, and  $\theta_x$  and  $\theta_y$  are the phases of the  $x$ - and  $y$ - components of the polarized radiation. For circular polarization, frequency and amplitude are equal for both  $(x, y)$  polarization directions and the phases are  $(\theta_x = 0, \theta_y = \pi/2)$  for a left circularly polarized pulse (LCP) and  $(\theta_x = \pi/2, \theta_y = 0)$  a right circularly polarized pulse (RCP).

Since the dipole operator  $\hat{\mu}_{x(y)}$  corresponds to the sum of the charges times their position, for the planar ring system (cf. Fig. 1) it reads

$$\hat{\mu}_x = -eR \sum_{s=0}^{n-1} \cos(\varphi_s) |\chi_s\rangle \langle \chi_s| \tag{9}$$

$$\hat{\mu}_y = -eR \sum_{s=0}^{n-1} \sin(\varphi_s) |\chi_s\rangle \langle \chi_s|, \tag{10}$$

and the light-matter interaction term reads  $-\vec{\hat{\mu}} \cdot \vec{E}(t)$ . Let us now consider, for example, the dipole

interaction for LCP light:

$$\vec{\hat{\mu}} \cdot \vec{E}(t)|_{\text{LCP}} = \varepsilon (\hat{\mu}_x \cos(\omega t) - \hat{\mu}_y \sin(\omega t)) \quad (11)$$

$$= \frac{1}{2} \varepsilon ((\hat{\mu}_x + i\hat{\mu}_y) e^{i\omega t} + (\hat{\mu}_x - i\hat{\mu}_y) e^{-i\omega t}), \quad (12)$$

where the second line is reached using Euler's formula for the cosine and sine functions. For resonant, one-photon absorption from a weakly interacting field one can apply the standard rotating wave approximation and keep only the energy-conserving term proportional to  $e^{i\omega t}$  to reach

$$\vec{\hat{\mu}} \cdot \vec{E}(t)|_{\text{LCP}} \approx \frac{1}{2} \varepsilon \hat{\mu}_+ e^{i\omega t}, \quad (13)$$

where we have defined  $\hat{\mu}_\pm = \hat{\mu}_x \pm i\hat{\mu}_y$ . The interaction with RCP light follows analogously substituting  $\hat{\mu}_-$  in Eq. (13). Finally, combining the definition of  $\hat{\mu}_\pm$  with Eqs. (9, 10) one can write

$$\hat{\mu}_\pm = -eR \sum_{s=0}^{n-1} e^{\pm i\varphi_s} |\chi_s\rangle \langle \chi_s|. \quad (14)$$

Applying operator (14) to the eigenstates in Eq. 2, corresponding to a one-photon interaction, results in  $\hat{\mu}_+ |\phi_k\rangle = -eR |\phi_{k+1}\rangle$  for LCP and  $\hat{\mu}_- |\phi_k\rangle = -eR |\phi_{k-1}\rangle$  for RCP light. Starting from the ground electronic state  $|\phi_0\rangle$ , LCP light thus populates the  $|\phi_1\rangle$  state whereas RCP light populates  $|\phi_{-1}\rangle$ . All other excited electronic states with  $|k| > 1$  are dark, i.e. they cannot be reached through a one-photon transition from the ground state.

In the  $|\phi_{(1,-1)}\rangle$  states, the circulation direction of the electrons along the ring is the same as the rotation direction of the circularly polarized electromagnetic fields that induced the electronic transition. We refer to such a pair of degenerate electronic states as *regular current* states in opposition to *inverse current* degenerate pairs introduced in the following.

*Inverse ring current* – The  $n$ -fold symmetry of an  $n$ -sites ring can be frustrated by the addition

of an  $m$ -fold-symmetry perturbing potential defined at the discrete angles  $\varphi_s$  as

$$\hat{V} = \lambda \sum_{s=0}^{n-1} \cos(m\varphi_s) |\chi_s\rangle \langle \chi_s|, \quad (15)$$

where  $m < n$  and  $m$  is a divisor of  $n$ . For example, the  $m = 1$  case lowers the symmetry of the rotational axis to  $C_1$ , meaning that all sites have a different energy, and all degeneracies are lifted. The  $m = 2$  case also lifts all degeneracies by lowering the symmetry of the rotational axis to  $C_2$ . The  $m \geq 3$  case preserves enough symmetry and doubly-degenerate states still exist. Chemically, such a symmetry-lowering potential corresponds to introducing different atom types or chemical residues along the ring.

As an example, one can consider the case with  $(n, m) = (6, 3)$  in Fig. 1 (c) and (d). The six-membered ring may correspond to a tight-binding (or Hückel) model of benzene ( $C_6H_6$ ). The  $m = 3$  potential lowers the symmetry of the rotational axis from  $C_6$  to  $C_3$ , for example in the 1,3,5-triazine molecule ( $C_3N_3H_3$ ) where three (CH) groups are substituted by the isoelectronic N atom.

The  $2\pi/m$ -periodic perturbing potential introduced by the different atom types along the ring couples the  $k$ -basis states according to the matrix elements

$$\langle \phi_k | \cos(m\varphi_s) | \phi_{k\pm m} \rangle = 1, \quad (16)$$

and zero otherwise, which follows from inserting  $\cos(m\varphi_s) = (\exp(im\varphi_s) + \exp(-im\varphi_s))/2$ . Therefore, continuing with the (6, 3) example, the perturbing potential couples the momentum state  $k = 1$  with the state  $k = -2$ , where the former is bright to LCP and the latter is dark. Considering first-order perturbation theory for these two states yields

$$\begin{aligned} |\tilde{\phi}_a^{(L)}\rangle &= |\phi_1\rangle - \frac{\lambda}{2t} |\phi_{-2}\rangle \\ |\tilde{\phi}_b^{(L)}\rangle &= |\phi_{-2}\rangle + \frac{\lambda}{2t} |\phi_1\rangle \end{aligned} \quad (17)$$

(in intermediate normalization) with second-order corrected energies  $E_a = -t - \frac{\lambda^2}{2t}$  and  $E_b = t + \frac{\lambda^2}{2t}$ . The  $(L)$  superscript indicates that both states in Eq. (17) are populated by LCP light absorption starting from the ground electronic state, since both have a contribution from the basis state  $|\phi_1\rangle$ .

The key difference lies in the expectation value of the electronic angular momentum for both perturbed states

$$\begin{aligned}\langle \tilde{\phi}_a^{(L)} | \hat{l}_z | \tilde{\phi}_a^{(L)} \rangle &= L_{1,1} + \frac{\lambda^2}{4t^2} L_{-2,-2} \approx L_{1,1} \\ \langle \tilde{\phi}_b^{(L)} | \hat{l}_z | \tilde{\phi}_b^{(L)} \rangle &= L_{-2,-2} + \frac{\lambda^2}{4t^2} L_{1,1} \approx L_{-2,-2}.\end{aligned}\quad (18)$$

$|\tilde{\phi}_a^{(L)}\rangle$  is a *regular current* state in the sense indicated above. We are now ready to introduce the main definition of this paper.  $|\tilde{\phi}_b^{(L)}\rangle$  is an *inverse current* state: it is reached from the ground electronic state by interaction with LCP light, yet the electrons circulate in opposite direction to the rotation of the electromagnetic radiation fields that set them in motion. The same argument can be made for the  $|\tilde{\phi}_a^{(R)}\rangle$  and  $|\tilde{\phi}_b^{(R)}\rangle$  states, which are energy-degenerate with the  $|\tilde{\phi}_a^{(L)}\rangle$  and  $|\tilde{\phi}_b^{(L)}\rangle$  states, respectively. Thus,  $|\tilde{\phi}_a^{(L/R)}\rangle$  constitute a *regular current* pair of degenerate electronic states, whereas  $|\tilde{\phi}_b^{(L/R)}\rangle$  constitute an *inverse current* pair.

*Definition:* A *regular current* state  $|\psi_{\text{reg}}\rangle$  fulfills

$$\langle \phi_0 | \hat{\mu}_+ | \phi_{\text{reg}} \rangle \neq 0 \quad \text{and} \quad \langle \phi_{\text{reg}} | \hat{l}_z | \phi_{\text{reg}} \rangle > 0 \quad (19)$$

or

$$\langle \phi_0 | \hat{\mu}_- | \phi_{\text{reg}} \rangle \neq 0 \quad \text{and} \quad \langle \phi_{\text{reg}} | \hat{l}_z | \phi_{\text{reg}} \rangle < 0.$$

An *inverse current* state  $|\phi_{\text{inv}}\rangle$  fulfills

$$\langle \phi_0 | \hat{\mu}_+ | \phi_{\text{inv}} \rangle \neq 0 \quad \text{and} \quad \langle \phi_{\text{inv}} | \hat{l}_z | \phi_{\text{inv}} \rangle < 0 \quad (20)$$

or

$$\langle \phi_0 | \hat{\mu}_- | \phi_{\text{inv}} \rangle \neq 0 \quad \text{and} \quad \langle \phi_{\text{inv}} | \hat{l}_z | \phi_{\text{inv}} \rangle > 0$$

For all degenerate electronic-state pairs, either both states are regular, or both states are inverse. These definitions are fully general and not constrained to tight-binding models and one-electron wavefunctions, as will be discussed below. This definition is summarized in Table 1.

Table 1: Truth table specifying the definition of regular (R) and inverse (I) current states in a molecular system. The first row indicates the sign of the expectation value of the in-plane angular momentum of the electrons,  $\hat{l}_z$ . The first column indicates whether the corresponding excited electronic state is reached from the ground state via the  $\hat{\mu}_+$  or  $\hat{\mu}_-$  transition dipole operator.

$\hat{\mu}_\pm \backslash \hat{l}_z$	+	-
+	R	I
-	I	R

Summarizing, ring-shaped systems of  $m$ -fold symmetry originating from a higher frustrated  $n$ -fold symmetry feature inverse current states belonging to an  $E$  symmetry representation. The  $m$ -fold perturbation potential mixes the bright  $k = \pm 1$  basis states with contributions of higher  $|k|$  with the *opposite* circulation direction. In the higher-energy degenerate pair, the current component with inverse direction has the largest weight and the resulting states are of inverse type.

*Independent-electron model* – After having presented the theory for regular and inverse current states in the one-electron periodic tight-binding Hamiltonian, we now generalize it to the many-body case, first without electron-electron interactions, and thereafter considering them. Introducing the Fermionic creation (annihilation) operators  $\hat{a}_s^\dagger$  ( $\hat{a}_s$ ) for localized site  $s$ , the Hamiltonian now reads

$$\hat{H} = -t \sum_{s=0}^{n-1} \sum_{\sigma=\alpha,\beta} \left( \hat{a}_{s,\sigma}^\dagger \hat{a}_{s+1,\sigma} + \text{h.c.} \right) + \sum_{s=0}^{n-1} \sum_{\sigma=\alpha,\beta} V_s \hat{a}_{s,\sigma}^\dagger \hat{a}_{s,\sigma} \quad (21)$$

where  $t$  is as before the hopping integral. We consider tight-binding models for the  $\pi$  orbitals of  $C_6H_6$  and  $C_3N_3H_3$ , where  $V_s = 0$  and  $V_s = \lambda \cos(3\varphi_s)$ , respectively. In our numerical calculations, we have utilized the parameter values  $t = 0.0918$  au and  $\lambda = 0.75t$ .<sup>26,27</sup>

We assume the molecules to lie in the  $xy$ -plane and consider the  $C_6$  and  $C_3$  point groups in the discussion, as the full labelling of the  $D_{6h}$  and  $D_{3h}$  groups is not needed. Under the  $C_6$  group, the

transition dipole for radiation polarized in the  $xy$ -plane transforms as the  $E_1$  representation, with the electronic states of the group spanning the representations

$$\Gamma_{C_6H_6} = A \oplus E_1 \oplus E_2 \oplus B. \quad (22)$$

Consequently, within the tight-binding model, the electronic absorption spectrum (cf. Fig. 2a) features a single peak at 5 eV with two-fold degeneracy, as indicated in Fig. 3. The corresponding angular momentum  $\langle \hat{l}_z \rangle / 2\hbar d$  of this state, reached through absorption of one LCP photon, is shown with orange trace. Similarly, the representation of the electronic states of the  $C_3N_3H_3$  model system under the  $C_3$  symmetry (cf. Fig. 1d) reads

$$\Gamma_{C_3N_3H_3} = 2(A \oplus E), \quad (23)$$

and now the transition dipole in the  $xy$ -plane transforms as  $E$ . The higher-energy electronic states, belonging to the  $E_2$  representation in benzene, belong to the  $E$  representation after the triple (CH) $\rightarrow$ (N) substitution. The transition to the higher energy  $E$  band becomes dipole allowed and a new line of small intensity is visible in the electronic absorption spectrum, Fig. 2b, and indicated in the energy-levels scheme in Fig. 3 by the transitions to the higher-energy  $E$  states. As illustrated by the orange traces indicating the expectation value of the angular momentum operator, Eq. (4), this optically-active state is of inverse ring current character. This inverse character is due to the mixing of opposite angular momentum states through the perturbing potential of lower symmetry, as described in Eq. (18).

*Electron correlation* – Before turning to the *ab initio* results, we consider the effect of correlation in the angular momentum of the electrons by introducing a Hubbard electron-repulsion term between  $\alpha$  and  $\beta$  electrons on the same site,

$$\hat{U} = \varepsilon \sum_s \hat{a}_{s,\alpha}^\dagger \hat{a}_{s,\alpha} \hat{a}_{s,\beta}^\dagger \hat{a}_{s,\beta}, \quad (24)$$

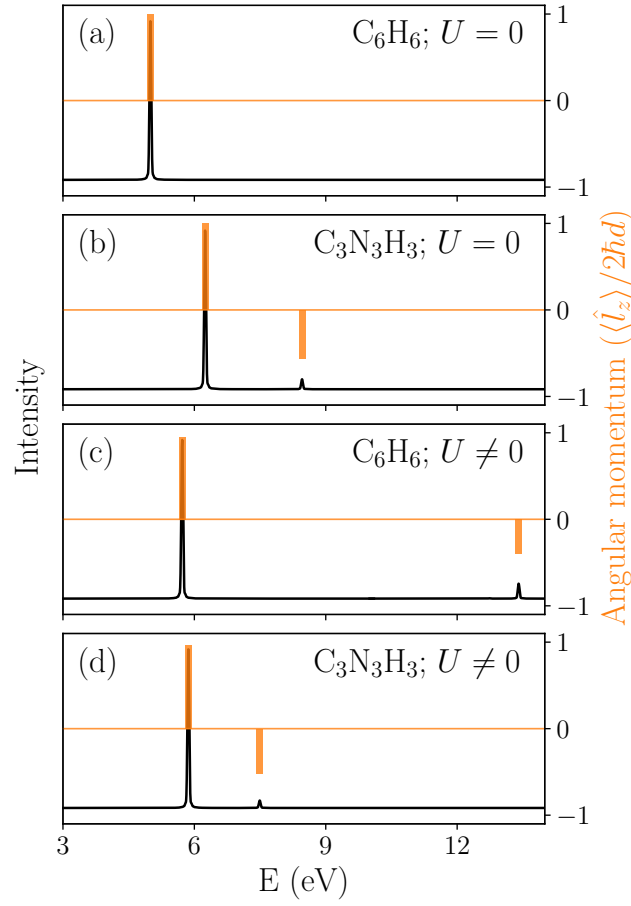


Figure 2: Electronic spectrum (in black) and the corresponding angular momentum (in orange) of the states reached through the absorption of one LCP photon in the tight-binding models of  $C_6H_6$  and  $C_3N_3H_3$  systems. Panels (a/b) depict results without electron correlation effects, while panels (c/d) include the effects of electron correlation.

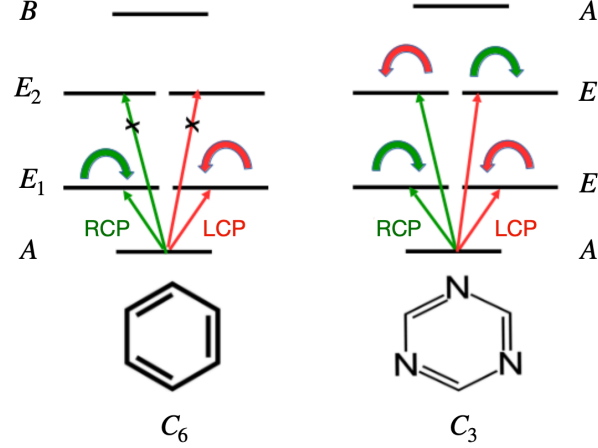


Figure 3: Independent-electron model transitions for benzene and sym-triazine. Red and green lines indicate the absorption of LCP and RCP photons, respectively, and the curly arrows represent electron circulation direction in the corresponding  $E$  states. In benzene, the  $A \rightarrow E_1$  electronic transition, dipole-allowed due to  $C_6$  symmetry, leads to a single peak in the absorption spectrum. Symmetric (CH)  $\rightarrow$  (N) substitution reduces symmetry to  $C_3$  in symm-triazine, altering the spectrum with a second peak at higher energy, where electronic circulation is in the opposite direction of the absorbed CP field.

to the tight-binding model in Eq. 21. As with the perturbing potential, the on-site repulsion can mix the angular momentum eigenstates even within the  $C_6H_6$  system. This can be seen by transforming the  $\hat{U}$  operator in the local basis to the  $k$ -basis using Eq. (2),

$$\hat{U} = \frac{\varepsilon}{n^2} \sum_{s=0}^{n-1} \sum_{k_1, k_2, k_3, k_4} e^{i\Delta k \varphi_s} \hat{b}_{k_1, \alpha}^\dagger \hat{b}_{k_2, \alpha} \hat{b}_{k_3, \beta}^\dagger \hat{b}_{k_4, \beta}, \quad (25)$$

where  $\Delta k = k_2 + k_4 - k_1 - k_3$  and  $\varphi_s = \frac{2\pi}{n}s$ .  $\hat{b}_{k, \sigma}^\dagger$  ( $\hat{b}_{k, \sigma}$ ) create (annihilate) a  $\sigma$ -spin electron with  $k$  momentum.

The absorption spectrum for the  $C_6H_6$  model is shown in Fig. 2c, where a peak of small intensity and inverted character appears in the high-energy edge of the spectrum. As Eq. (25) indicates, the electron-electron correlation mixes the  $k$ -states of the one-electron basis, i.e. electrons can exchange angular momentum via their Coulomb interaction, and thus inverted current states can occur. Thus, as this simple example illustrates, inverted current states can exist on the basis of electron correlation only. Figure 2d illustrates the absorption spectrum for the  $C_3N_3H_3$  with elec-

tronic correlation. Again, an inverse-current line is present in the absorption spectrum. In this case though, it is not possible to decide which of the mechanisms, scattering of the electrons against a symmetry-lowering, perturbing potential or electron-electron correlation, is primarily responsible for the inverse current states.

*Ab initio calculation* – Until now, we used tight-binding models of C<sub>6</sub>H<sub>6</sub> and C<sub>3</sub>N<sub>3</sub>H<sub>3</sub> to investigate the origin of the inverse ring currents on the basis of symmetry lowering and electron correlation effects. This offered much insight into the fundamental origin of this phenomenon but the question arises, whether inverse current states can be identified from *ab initio* calculations of excited electronic states in ring-shaped molecules.

To identify whether a doubly degenerate  $E$  state of a planar molecule lying on the  $xy$ -plane exhibits regular or inverse current behavior, the following matrix elements, which can be obtained from *ab initio* calculations are necessary and sufficient:

$$\langle \psi_m | \hat{\mu}_{x/y} | \psi_0 \rangle = \mu_{x/y}^{m0}, \quad (26)$$

and

$$\langle \psi_m | \frac{\partial}{\partial \varphi} | \psi_n \rangle = D_{m,n}, \quad (27)$$

where,  $|\psi_{m,n}\rangle$  ( $m, n = \{1, 2\}$ ) are the two degenerate and real orthonormal wavefunctions of the  $E$  excited state and  $|\psi_0\rangle$  is the ground state wavefunction. Note that here we assume that the degenerate states obtained from an *ab initio* calculation are real, which is the most common situation. We make no assumptions either that the transition dipoles of the two real states are aligned with the spatial  $x$  and  $y$  axes, which is the case if no symmetry is used in the *ab initio* calculation.  $\mu_x^{m0}$  and  $\mu_y^{m0}$  correspond to the transition dipole moment between ground and excited  $E$  states along the  $x$  and  $y$  directions, respectively.  $D_{m,n}$  corresponds to the matrix elements of the differential operator between the degenerate  $E$  states, and is related to the angular momentum operator as  $L_{m,n} = -i\hbar D_{m,n}$ . For real wavefunctions,  $D_{1,1} = D_{2,2} = 0$ , and  $D_{1,2} = -D_{2,1}$ , in contrast with

Eq. (4), where the doubly-degenerate states are complex. One can form two complex wavefunctions of the  $E$  state from  $|\psi_1\rangle$  and  $|\psi_2\rangle$  as

$$\begin{aligned} |\psi_A\rangle &= \frac{1}{\sqrt{2}} (|\psi_1\rangle + i|\psi_2\rangle), \\ |\psi_B\rangle &= \frac{1}{\sqrt{2}} (|\psi_1\rangle - i|\psi_2\rangle). \end{aligned} \quad (28)$$

Now, to identify whether  $|\psi_A\rangle$  or  $|\psi_B\rangle$  is reached when the ground state absorbs a LCP photon, one needs to calculate the following matrix elements

$$\begin{aligned} \langle \psi_A | \hat{\mu}_\pm | \psi_0 \rangle &= \langle \psi_A | (\hat{\mu}_x \pm i\hat{\mu}_y) | \psi_0 \rangle \\ &= \frac{1}{\sqrt{2}} (\mu_x^{10} \pm \mu_y^{20}) - \frac{i}{\sqrt{2}} (\mu_x^{20} \mp \mu_y^{10}), \end{aligned} \quad (29)$$

and

$$\begin{aligned} \langle \psi_B | \hat{\mu}_\pm | \psi_0 \rangle &= \langle \psi_B | (\hat{\mu}_x \pm i\hat{\mu}_y) | \psi_0 \rangle \\ &= \frac{1}{\sqrt{2}} (\mu_x^{10} \mp \mu_y^{20}) + \frac{i}{\sqrt{2}} (\mu_x^{20} \pm \mu_y^{10}). \end{aligned} \quad (30)$$

There can only be two possibilities: (i) either  $\mu_x^{10} = \mu_y^{20}$  and  $\mu_x^{20} = -\mu_y^{10}$  or (ii)  $\mu_x^{10} = -\mu_y^{20}$  and  $\mu_x^{20} = \mu_y^{10}$ . Hence, when the ground state absorbs a LCP photon the system transitions to  $|\psi_A\rangle$  for the former, and to  $|\psi_B\rangle$  for the latter case. The expectation value of the angular momentum operator is given as

$$\begin{aligned} \langle \psi_A | \hat{l}_z | \psi_A \rangle &= D_{1,2}, \\ \langle \psi_B | \hat{l}_z | \psi_B \rangle &= -D_{1,2}. \end{aligned} \quad (31)$$

Finally, following the definitions (19) and (20), the degenerate  $E$  state is regular if the equivalent

conditions are fulfilled

$$\text{sgn}(\mu_x^{10} \cdot \mu_y^{20}) = \text{sgn}(D_{1,2}) \quad (32)$$

$$\text{sgn}(\mu_x^{20} \cdot \mu_y^{10}) = -\text{sgn}(D_{1,2}),$$

where  $\text{sgn}(x)$  is the sign of  $x$ . If the signs on the right-hand-side are reversed, the  $E$  state is an inverse ring current state.

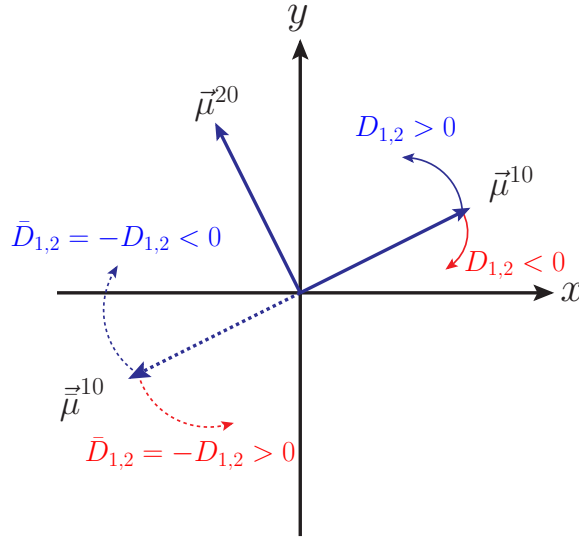


Figure 4: Schematic visualization of regular and inverse ring current states.

The process of identifying an  $E$  state as regular or inverse has been described above and is fully contained in the relations 32. Alternatively, it can be visualized by the scheme presented in Fig. 4. One starts by considering the vectors  $\vec{\mu}^{10}$  and  $\vec{\mu}^{20}$ , together with the sign of  $D_{1,2} = \langle \psi_1 | \partial_\phi | \psi_2 \rangle$ . If  $D_{1,2} > 0$ , we associate with it an anticlockwise rotation direction (angle grows); otherwise, this direction is clockwise. Following this direction, if the path from  $\vec{\mu}^{10}$  to  $\vec{\mu}^{20}$  is the shortest, i.e.,  $90^\circ$  (indicated by the blue arrow), the corresponding  $E$  state is regular. Alternatively, if the path from  $\vec{\mu}^{10}$  to  $\vec{\mu}^{20}$  covers  $270^\circ$  (indicated by the red arrow), the  $E$  state is inverse. This conclusion remains unaltered when introducing an arbitrary phase factor (-1) to one of the calculated  $E$  states ( $\psi_1$  in the figure:  $|\bar{\psi}_1\rangle = -|\psi_1\rangle$ ). Both the transition dipole,  $\vec{\bar{\mu}}^{10} = -\vec{\mu}^{10}$  (indicated by the dashed vector), and the derivative operator matrix elements,  $\bar{D}_{1,2} = -D_{1,2}$  (indicated by the dashed arrow),

change their sign while the conditions 32 and their graphical interpretation remain unaltered.

For the numerical calculation of benzene and sym-triazine, the geometry is optimized at the B3LYP/cc-pVDZ label of theory and the molecular orbitals (MO) are calculated using the cc-pVDZ basis for H, C, and N atoms. The electronic states are calculated using configuration interaction with single and double excitation (CISD) within an orbital space where the 6 lowest core MOs are frozen and the next 30 spatial MOs are active. In Table 2, we present the transition dipole moment between various doubly degenerate electronic states and ground state, the expectation value of the angular momentum operator along the z-direction of benzene and 1,3,5-sym triazine molecules, and identify the inverse ring current states among these electronic subspaces.

Table 2: Transition dipole moment (TDM) and angular momentum expectation values in different electronic sub-spaces of benzene and sym-triazine calculated at the CISD/cc-pVDZ level of theory. ‘States’, indicates the excitation energy (in eV) of the corresponding degenerate state and its symmetry representation.  $E_+$  and  $E_-$  represent the excited degenerate wavefunctions reached by absorption of a LCP and RCP photon, respectively. ‘Type’ indicates whether the corresponding electronic manifold state is regular (R) or inverse (I).

Molecule	States	TDM	$\langle E_{\pm}   \hat{l}_z   E_{\pm} \rangle$	Type
benzene	$1E_{1u}(10.82)$	1.97	$\pm 0.65$	R
	$2E_{1u}(15.39)$	1.09	$\mp 1.83$	I
	$3E_{1u}(16.52)$	1.09	$\pm 0.13$	R
	$4E_{1u}(17.07)$	1.05	$\pm 1.16$	R
	$5E_{1u}(18.69)$	0.86	$\pm 0.39$	R
sym-triazine	$1E'(11.76)$	1.38	$\pm 0.53$	R
	$2E'(12.89)$	0.70	$\mp 0.69$	I
	$3E'(13.79)$	0.06	$\pm 0.78$	R
	$4E'(14.36)$	0.41	$\mp 0.95$	I
	$5E'(15.89)$	0.28	$\pm 0.15$	R

*Conclusions* – In this work, we have investigated the possibility to have electronic states with inverse ring currents on a purely electronic basis, i.e. without vibronic coupling effects and for clamped nuclei. Such inverse ring current states correspond to a doubly degenerate manifold in which electrons circulate in opposite direction to the rotation of electromagnetic fields that set them in motion. The existence of inverse ring currents state within fixed nuclei can be attributed

to two factors: (i) the scattering of electrons with the discrete sites of an  $n$ -fold symmetry planar ring system, (ii) electron correlation effects. To demonstrate the former effect, we considered an independent electron model, where the inverse ring current states emerge when the symmetry is lowered from  $n$  to  $n/2$ , for example by substitution with hetero-atoms. The effect of electron correlation was studied by introducing a Hubbard electron-electron repulsion term to the independent electron model. With electron correlation, inverse ring current states appear because the electrons can exchange angular momentum via their Coulomb interaction.

Finally, we have outlined a simple procedure to identify inverse ring current states from *ab initio* calculations. As a proof-of-concept, this was illustrated with CISD calculations of the benzene and sym-triazine molecules, which demonstrate the existence of inverse ring current manifolds for clamped nuclei, as predicted as well by a tight-binding model. A more systematic characterization of inverse ring current manifolds in larger and more complex molecules such as Mg-porphyrin,<sup>28</sup> large heteropolycyclic molecules, or pure carbon cycles like C<sub>18</sub>,<sup>29</sup> while using more accurate excited-state electronic structure methods, will be the subject of future investigations.

## Acknowledgement

KRN and OV acknowledge the collaborative research center “SFB 1249: N-Heteropolyzyklen als Funktionsmaterialien” of the German Research Foundation (DFG) for financial support.

## References

- (1) Barth, I.; Manz, J.; Shigeta, Y.; Yagi, K. Unidirectional electronic ring current driven by a few cycle circularly polarized laser pulse: quantum model simulations for Mg- porphyrin. *J. Am. Chem. Soc.* **2006**, *128*, 7043–7049.
- (2) Barth, I.; Manz, J. Periodic electron circulation induced by circularly polarized laser pulses: quantum model simulations for Mg Porphyrin. *Angew. Chem. Int. Ed.* **2006**, *45*, 2962–2965.
- (3) Barth, I.; Manz, J. Electric ring currents in atomic orbitals and magnetic fields induced by short intense circularly polarized  $\pi$  laser pulses. *Phys. Rev. A* **2007**, *75*, 012510.
- (4) Barth, I.; Manz, J. *Progress in Ultrafast Intense Laser Science VI*; Springer, 2010; pp 21–44.
- (5) Ulusoy, I. S.; Nest, M. Correlated electron dynamics: How aromaticity can be controlled. *J. Am. Chem. Soc.* **2011**, *133*, 20230–20236.
- (6) Mineo, H.; Yamaki, M.; Kim, G.-S.; Teranishi, Y.; Lin, S. H.; Fujimura, Y. Induction of unidirectional  $\pi$ -electron rotations in low-symmetry aromatic ring molecules using two linearly polarized stationary lasers. *Phys. Chem. Chem. Phys.* **2016**, *18*, 26786–26795.
- (7) Mineo, H.; Fujimura, Y. Quantum design of  $\pi$ -electron ring currents in polycyclic aromatic hydrocarbons: parallel and antiparallel ring currents in naphthalene. *J. Phys. Chem. Lett.* **2017**, *8*, 2019–2025.
- (8) Mineo, H.; Fujimura, Y. Quantum control of coherent  $\pi$ -electron ring currents in polycyclic aromatic hydrocarbons. *J. Chem. Phys.* **2017**, *147*, 224301.

- (9) Liu, C.; Manz, J.; Ohmori, K.; Sommer, C.; Takei, N.; Tremblay, J. C.; Zhang, Y. Attosecond control of restoration of electronic structure symmetry. *Phys. Rev. Lett.* **2018**, *121*, 173201.
- (10) Kanno, M.; Kono, H.; Fujimura, Y. Laser-control of ultrafast  $\pi$ -electron ring currents in aromatic molecules: roles of molecular symmetry and light polarization. *Appl. Sci.* **2018**, *8*, 2347.
- (11) Pershin, Y. V.; Piermarocchi, C. Laser-controlled local magnetic field with semiconductor quantum rings. *Phys. Rev. B* **2005**, *72*, 245331.
- (12) Matos-Abiague, A.; Berakdar, J. Photoinduced charge currents in mesoscopic rings. *Phys. Rev. Lett.* **2005**, *94*, 166801.
- (13) Räsänen, E.; Castro, A.; Werschnik, J.; Rubio, A.; Gross, E. K. U. Optimal Control of Quantum Rings by Terahertz Laser Pulses. *Phys. Rev. Lett.* **2007**, *98*, 157404.
- (14) Anthony, J. E. Functionalized acenes and heteroacenes for organic electronics. *Chem. Rev.* **2006**, *106*, 5028–5048.
- (15) Kanno, M.; Kono, H.; Fujimura, Y.; Lin, S. H. Nonadiabatic response model of laser-induced ultrafast  $\pi$ -electron rotations in chiral aromatic molecules. *Phys. Rev. Lett.* **2010**, *104*, 108302.
- (16) Nandipati, K. R.; Vendrell, O. Dynamical Jahn-Teller effects on the generation of electronic ring currents by circularly polarized light. *Phys. Rev. Research* **2021**, *3*.
- (17) Yamaki, M.; Teranishi, Y.; Nakamura, H.; Lin, S. H.; Fujimura, Y. The generation of stationary  $\pi$ -electron rotations in chiral aromatic ring molecules possessing non-degenerate excited states. *Physical Chemistry Chemical Physics* **2016**, *18*, 1570–1577.
- (18) Kaiser, K.; Scriven, L. M.; Schulz, F.; Gawel, P.; Gross, L.; Anderson, H. L. An sp-hybridized molecular carbon allotrope, cyclo[18]carbon. *Science* **2019**, *365*, 1299–1301.

- (19) Bandrauk, A. D.; Chelkowski, S.; Nguyen, H. S. Attosecond localization of electrons in molecules. *Int. J. Quantum Chem.* **2004**, *100*, 834–844.
- (20) Krausz, F.; Ivanov, M. Attosecond physics. *Rev. Mod. Phys.* **2009**, *81*, 163.
- (21) Yuan, K.-J.; Shu, C.-C.; Dong, D.; Bandrauk, A. D. Attosecond dynamics of molecular electronic ring currents. *J. Phys. Chem. Lett.* **2017**, *8*, 2229–2235.
- (22) Nobusada, K.; Yabana, K. Photoinduced electric currents in ring-shaped molecules by circularly polarized laser pulses. *Phys. Rev. A* **2007**, *75*, 032518.
- (23) Yuan, K.-J.; Guo, J.; Bandrauk, A. D. Generation of ultrafast magnetic fields from molecular coherent electron currents. *Phys. Rev. A* **2018**, *98*, 043410.
- (24) Nandipati, K. R.; Vendrell, O. On the generation of electronic ring currents under vibronic coupling effects. *Chem. Phys.* **2020**, *153*, 224308.
- (25) Messiah, A. *Quantum mechanics*; Dover Publications: Mineola, N.Y, 1999.
- (26) Franco, I.; Rubio, A.; Brumer, P. Long-lived oscillatory incoherent electron dynamics in molecules: trans-polyacetylene oligomers. *New J. Phys.* **2013**, *15*, 43004–043004.
- (27) Li, M.; Lin, X. Adapted Su-Schrieffer-Heeger Hamiltonian for polypyrrole. *Phys. Rev. B Condens. Matter* **2010**, *82*, 155141.
- (28) Mai, S.; González, L. Molekulare Photochemie: Moderne Entwicklungen in der theoretischen Chemie. *Angew. Chem.* **2020**, *132*, 16976–16992.
- (29) Diederich, F.; Rubin, Y.; Knobler, C. B.; Whetten, R. L.; Schriver, K. E.; Houk, K. N.; Li, Y. All-Carbon Molecules: Evidence for the Generation of Cyclo[18]carbon from a Stable Organic Precursor. *Science* **1989**, *245*, 1088–1090.